NASA CR-172,135

NASA Contractor Report 172135

NASA-CR-172135
19830024949

STRESSES IN A QUASI-ISOTROPIC PIN LOADED CONNECTOR USING PHOTOELASTICITY

M. W. Hyer and D. H. Liu

VIRGINIA POLYTECHNIC INSTITUTE AND STATE UNIVERSITY
Department of Engineering Science and Mechanics
Blacksburg, Virginia 24061

Grant NSG-1621
August 1983

National Aeronautics and
Space Administration

Langley Research Center
Hampton, Virginia 23665

INTRODUCTION

The concept of using birefringent fiber-reinforced materials as a tool for the stress analysis of composites has been discussed by various investigators [1-5]. The hoop stresses around an elliptical hole in a tensile strip were studied by Prabhakaran and Dally [6] using the birefringent fiber-reinforced materials. Residual stresses in filament-wound rings were studied by Knight [7]. Prabhakaran [8] used the phenomenon to investigate stresses on the inner and outer boundaries of an orthotropic ring. Several other problems which have been examined with the technique were discussed by Daniel [9]. The shear difference method was introduced by Knight and Pih [10] as a way to separate the stresses in a tensile strip with a central circular hole. They studied the stresses at the net section and at several other locations and found good agreement with finite element results. Stresses in an individual lamina in a $[\pm 30]_S$ tensile strip were measured by Voloshin [11] using a reflective coating between lamina. Recently, the isochromatic fringe patterns and the shear-out stresses in a pin-loaded connector made of birefringent fiber-reinforced material were presented by Prabhakaran [12].

This paper presents further photoelastic results regarding the stresses in a pin-loaded fiber-reinforced connector. The connector is a birefringent fiber-reinforced composite with a lay-up of $[0_4/+45_4/-45_4/90_4]_S$, a quasi-isotropic configuration. This paper discusses the details of the connector and how it was loaded. The contact stresses between the pin and the hole edge, as well as the hoop stresses, net-section stresses, and other pertinent stresses, were computed using an overdetermined finite-difference representation of the plane-

stress equilibrium equations. This method of stress separation is discussed and experimentally computed stresses presented. The results are compared with the results of other investigators.

The work reported herein was financially supported by the Structures Laboratory USARTL (AVRADCOM). The grant monitor was Donald J. Baker, Structures Laboratory, USARTL (AVRADCOM).

MODEL AND LOADING

Figure 1 shows the dimensions of the connector and the method of transferring loads into it. The connector was 203 mm (8.00 in.) wide and was made from a flat sheet of material fabricated by IITRI [13]. The material was glass-epoxy and was 2.29 mm (0.090 in.) thick. The fiber volume fraction of the material was approximately 50 percent. A complete description of the fiber and epoxy constituents, and the fabrication technique can be found in [13]. The fibers in the quasi-isotropic lay-up were aligned with the long direction of the connector, the width direction, and at $\pm 45°$ with these directions. The pin loading the hole was steel and was 50.8 mm (2.00 in.) in diameter. The pin was a clearance fit, requiring a slight amount of finger pressure to push it into the hole. It was felt this large a diameter was necessary if the fringes, and thus the stresses, around the hole were to be resolved accurately. With the geometry shown, the connector-width to hole-diameter ratio, W/D, was 4 and the end-distance to hole-diameter ratio, e/D, was 2.

The prime purpose of the model was to determine stresses at the net section and around the lower portions of the hole. No attempts were made to react the pin load and still have a full field view of the con-

nector. The steel yoke and crossbar were 6.35 mm (0.25 in.) thick and were joined together with pins. The system was loaded by a deadweight load, P, applied through pins at the far ends of the fixture. All pins in the loading mechanism were 9.84 mm (0.388 in.) in diameter. Aluminum doubler plates 3.17 mm (0.125 in.) thick were used to evenly distribute the concentrated load into the connector. The doublers transferred the load to the glass-epoxy through 10 small-diameter bolts.

The glass-epoxy material was cut to size using a diamond blade on a circular saw. The large hole in the connector was drilled using an ultrasonic core drill. Both the cutting and drilling operations used a liquid coolant. Fortunately, neither operation took much time and so there was no apparent degradation of the epoxy from the water-based coolants.

Disks, tensile strips, and four-point bend specimens cut from the material indicated the material was optically isotropic with a stress-optic constant, f, of 92.9 kPa/fringe/m (530 psi/fringe/in.). There was no evidence of residual birefringence. Young's modulus of the material was 23 GPa (3.4×10^6 psi). The ratio of pin modulus to connector modulus was 8.8 : 1, therefore the pin was considered to be rigid.

The stress-optic laws in a form useful for computing the stresses are:

$$\sigma_1 - \sigma_2 = fN \cos(2\theta) \tag{1}$$

$$\tau_{12} = \frac{fN}{2} \sin(2\theta) \ . \tag{2}$$

The stresses σ_1 and σ_2 are normal stresses in some orthogonal coordinate system in the plane of the connector and τ_{12} is the shear stress in that

system. In eqs. 1 and 2, neither the 1 axis nor the 2 axis are intended to be aligned with any particular direction on the connector. Later the 1 axis and 2 axis will be aligned with the x and y axes of fig. 1 and a polar coordinate system around the hole. The variable N is the isochromatic fringe number and θ is the optical isocline. The value of θ is measured positive from the +1 axis. Since the material was optically isotropic, and since there was no residual birefringence, the optical isocline is the principal stress direction relative to the +1 axis.

SEPARATION OF STRESSES

Equations 1 and 2 do not provide enough information to uniquely determine the stresses at each point in the connector. Separation of stresses was accomplished here by using the plane-stress equilibrium equations, in finite-difference form, as auxiliary conditions the stresses σ_1, σ_2 and τ_{12} had to satisfy. Since there are two equilibrium equations, the finite-difference representation of the equilibrium conditions and eqs. 1 and 2 resulted in four algebraic equations from which to compute the three stresses at a point. In addition, there were boundary conditions to impose on the stresses. The result was an overdetermined set of equations from which to determine the streses. Berghaus [14] addressed such a problem and his solution technique is used here. Voloshin [11] used a similar technique but incorporated the compatibility equations into the scheme as additional equations to be satisfied. Chandrashekhara and Jacob [15] used only the compatibility equations, and the appropriate boundary conditions, for stress separation.

In addition to the overdetermined approach, another approach was incorporated in the separation of stresses. This was to separate the

stresses in a zone-by-zone fashion over the area of the model. This approach is shown in figs. 2 and 3. These figures show the grids used for the finite-difference representation of the equilibrium equations. One grid system was a rectangular system and the other grid system was polar. Each grid system was broken into zones, the zones being numbered 1-11. The value of N and θ for use in eqs. 1 and 2 were measured experimentally at each grid point location and ultimately three stresses at each grid point were calculated. With this finite-difference scheme, the stresses were calculated in zone 1 first, then zone 2, etc. until stresses were finally calculated in zone 11.

For zone 1, the boundary conditions enforced were the traction-free conditions along the right edge and the bottom edge. For zone 2 the boundary conditions were the traction free conditions along the right edge and the stresses along the boundary between zones 1 and 2 as determined from the zone 1 calculations. This interfacing of zones continued up to zone 9. For polar zone 10, conditions along the outer circumferential boundary were determined by interpolation from zones 3, 5 and 6 calculations. Finally, zone 11 calculations used interpolated data on the outer circumferential boundary and zone 10 data along the radial interface with that zone.

The accuracy of the finite-difference scheme was checked before it was used with actual experimental data. This allowed for an assessment of the fineness of the mesh required. The check on the scheme was as follows: Bickley [16] presented the elasticity solution for an infinite isotropic plate loaded through a hole. The hole loading was a known radial traction felt to represent the effects of a pin in the hole. With the solution, the stresses in the infinite plate could be determined.

In the work here a rectangular area around the hole, of the size of the connector being studied, was isolated from the infinite plate. The proper tractions were applied at the edges of this rectangular area so the region of the infinite plate outside this rectangular area could be eliminated. The stress-optic laws were used in conjunction with Bickley's elasticity solution to compute a value of N and θ at each grid point on the grids of figs. 2 and 3. These values of N and θ were used as 'experimental data' in the overdetermined finite-difference scheme. Instead of traction-free boundary conditions, the normal and shear edge tractions necessary for isolating the rectangular area were used as boundary conditions for the finite-difference solution. The stresses from the finite-difference calculations were compared with the elasticity solution stresses. After several refinements of mesh size, the largest difference between the exact elasticity solution stresses and the finite-difference calculations was 3.5%. This occurred at the net-section hole edge. Thus the stress separation scheme was considered valid.

The fringes in orthotropic photoelastic materials are not generally as sharp and distinct as they are in commonly available isotropic photoelastic materials. In the actual experiment the fringes are recorded photographically using a high contrast negative film. The N and θ values at each grid point are determined from enlarged projections of these high contrast negatives. This method proved quite effective for an accurate determination of the isoclines around the hole. Actually the zones extended over the entire lower half of the model, not just the right hand portion, as implied by figs. 2 and 3. Slight asymmetries or differences in the isochromatic and isoclinic fringe patterns between

the left and right halves of the model prompted a stress analysis of both halves. Why the differences in the fringe patterns existed was not clear but slight inhomogeneities in the material were probably to blame. The loading fixture was checked for slight misalignments but none were found. The stress results presented are the average of the left and right side stresses.

The zone scheme was adapted originally to keep the number of algebraic equations in the overdetermined scheme to a reasonable number. However, it proved to be a convenient method for refining the mesh size from location to location on the model and for checking data reduction for consistency in a methodical, step-by-step fashion. An example of this is as follows. Referring to fig. 2, for any horizontal line across the width of the specimen below the hole,

$$\int_{x=-W/2}^{+W/2} \sigma_y dx = 0. \tag{3}$$

This particular integral of the stress is zero because the hole reacts all the pin load. There is no net reaction between the hole and the free end of the connector. The stresses were computed in zone 1 and the condition of eq. 3 was checked. If eq. 3 was not satisfied to within a certain tolerance, experimental data were checked for errors. When eq. 3 was satisfied, calculations proceded to zone 2. Of course, above the net section,

$$t \int_{x=-W/2}^{W/2} \sigma_y dx = P, \tag{4}$$

where t is the connector thickness. In the next section, numerical values of these integrals are reported.

EXPERIMENTAL RESULTS

Figure 4 shows a whole field view of the isochromatic fringe patterns in the connector. The applied load is 7700 N (1730 lb.). Figure 5 shows the 20° isocline near the hole. Figure 4 was taken using normal film while fig. 5 was taken using high contrast film.

The radial compressive stresses, σ_r, around the hole edge are shown in fig. 6. The stresses have been nondimensionalized by the bearing stress, S, which is defined to be

$$S = \frac{P}{Dt} , \tag{5}$$

All stresses shown in these and future figures were computed with a load, P, of 7700 N (1730 lb.) applied to the model. These and other results are the average of the left and right sides of the connector stresses. The results of several other investigators are superposed on the figure. The geometries of the connectors studied by the other investigators were not identical to the geometry studied here. The geometries of the various studies are noted on the figure.

Nisida, et al. [17] measured the stresses around a pin-loaded isotropic connector using a combination of photoelasticity and interferometry. Their measurements were purely experimental, requiring no auxiliary numerical condition. Crews et al. [18] assumed an elastic frictionless pin in his finite element analysis of a quasi-isotropic connector. De Jong [19] used an elasticity solution, assuming a rigid frictionless pin for his analysis of an infinite quasi-isotropic plate. The $\frac{4}{\pi} \cos \theta$ radial contact stresses distribution was assumed by Bickley and subsequently by many other workers. The simple $\frac{4}{\pi} \cos \theta$ radial stresss

distribution is quite close to all others, be they experimental, numerical, or analytical. Figure 7 shows the circumferential or hoop stress, σ_θ, at the hole edge. In addition, the results of other investigators are indicated on the figure. The stresses from ref. 16 are generated by the $\frac{4}{\pi}\cos\theta$ radial distribution on an infinite plate.

Figure 8 shows the net-section σ_y stresses. As can be seen, for this particular model geometry, the stress concentration factor, based on bearing stress, is 1.11. There is not much data for the net-section stresses, either numerical or experimental. De Jong [20] used a superposition of solutions to correct infinite plate solutions for finite width effects. These results are shown in fig. 8. Crews et al. computed a stress concentration factor at the hole edge of 1.25. Figure 9 shows the variation of the so-called shear-out stress. The shear-out stress is the shear stress τ_{xy} below the hole along the line from the net-section hole edge to the bottom free edge. Crews, et al. calculated this shear stress in their study and the results are shown in fig. 9.

As mentioned previously, eqs. 3 and 4 were used to gage the consistency and accuracy of the photoelastic stress calculations. Operationally, eqs. 3 and 4 were evaluated using Simpson's rule. Table 1 indicates the numerical value of the integrals for the horizontal locations A-A, B-B, C-C, and D-D shown in fig. 2. To form a measure of error, the numerical values of the integrals were divided by the load, P, applied to the model when the stresses were computed. This quotient, when compared to the ideal, was felt to be a measure of accuracy and reliability. As can be seen from Table 1, the integrals were within 3.6% of the ideal case.

Table 1
Value of Stress Integrals

horizontal location	ideal value	actual value	$\frac{\text{actual value}}{P}$
A-A	0	123 N (27.7 lb)	0.016
B-B	0	84 N (19.0 lb)	0.011
C-C	0	60.6 N (269 lb)	0.035
D-D	7700 N (1730 lb)	7975 N (1793 lb)	1.036

DISCUSSION

The experimental data presented here are somewhat unique. For the particular problem studied, very little experimental data exist. The vast majority of the work has been numerical or analytical. These data provide a comparison for numerical investigations. In addition, orthotropic photoelastic materials have not been used to any great extent to solve a problem of practical importance. The pin-loaded connector is a problem of importance in composite material mechanics and the application of the material to the problem studied here emphasizes the potential of the material.

The stresses presented herein are considered to be quite accurate. The numbers in Table 1 confirm that the stresses computed are at least globally consistent. The only difficulty encountered in the experiments was at the net section. Even without much load on the connector, small cracks formed in the 90° plys. The cracks were radial and coincident with the net section. These cracks did not appear to affect light transmission. However, there was a small amount of residual birefringence in the vicinity of the net section. Careful scrutiny around the remainder of the hole circumference indicated there was no residual birefringence elsewhere. This residual birefringence undoubtedly affected the value of N and θ. No adjustments were made for

this residual birefringence at the net section and this could be responsible for what appears to be, a slight radial compressive stress at the net-section and above (see fig. 6).

One other comment regarding residual effects is in order. In previous studies [21] with a unidirectional material, residual birefringent effects did exist throughout the material. This was due presumably to the differences in the thermoelastic properties of the constituents, coupled with the slightly elevated temperature cure of the material. The quasi-isotropic material used here exhibited no residual birefringence in the material as a whole. It is hypothesised that the four fiber orientations, 0°, 90°, 45°, and -45° effectively eliminated residual effects. There were residual effects but they did not lead to net birefringence by the time the light had passed through all ply orientations.

CONCLUSIONS

From the work reported here several general and specific conclusions can be drawn. It can be concluded that:

1) the photoelastic response of transparent glass-epoxy material in a quasi-isotropic configuration can be used successfully to determine the stresses in complex problems;
2) the overdetermined finite-difference representation of the equilibrium equations, coupled with the zone-by-zone scheme, is an effective way to separate stresses; and,
3) fringe sharpening and enlargement by photographic methods helps considerably in resolving fringes in glass-epoxy.

For the specific problem studied it can be concluded that:

1) the numerical and analytical resuults of previous investigators compares favorably with experimental findings;
2) the net-section stress concentration factor, based on bearing stress, is about 1.1; and,
3) the $\frac{4}{\pi}\cos\theta$ distribution often used to represent the radial contact stresses is a good approximation for quasi-isotropic materials.

REFERENCES

1. Pih, H. and Knight, C. E. "Photoelastic analysis of anisotropic fiber reinforced composites," J. of Composite Materials, vol. 3, pp. 94-107, 1969.

2. Sampson, R. C. "A stress-optic law for photoelastic analysis of orthotropic composites," Experimental Mechanics, vol. 10, no. 5, pp. 210-215, 1970.

3. Dally, J. W. and Prabhakaran, R., "Photo-orthotropic-elasticity," Experimental Mechanics, vol. 11, no. 8, pp. 346-356, 1971.

4. Chaturvedi, S. K., "Fundamental concepts of photoelasticity for anisotropic composite materials," Int. J. Engineering Science, vol. 20, no. 1, pp. 145-147, 1982.

5. Prabhakaran, R., "Extension of oblique-incident method to photo-orthotropic elasticity," Experimental Mechanics, vol. 22, no. 12, pp. 462-467, 1982.

6. Prabhakaran, R. and Dally, J. W. "The application of photo-orthotropic elasticity," Journal of Strain Analysis, vol. 7, no. 4, pp. 253-260, 1972.

7. Knight, C. E., Jr. "Orthotropic photoelastic analysis of residual stresses in filament-wound rings," Experimental Mechanics, vol. 12, no. 2, pp. 107-112, 1972.

8. Prabhakaran, R. "Photoelastic analysis of an orthotropic ring under diametral compression," AIAA Journal, vol. 11, no. 6, pp. 777-778, 1973.

9. Daniel, I. M. "Photoelastic studies of mechanics of composites," Progress in Experimental Mechanics, Durelli Anniversary Volume, Catholic University of America, 1975.

10. Knight, C. E., Jr. and Pih, H. "Shear difference method and application in orthotropic photoelasticity," J. of Engineering Materials and Technology, (transactions of ASME), vol. 98, pp. 369-374, 1976.

11. Voloshin, A., "Stress field evaluation in photoelastic anisotropic materials: experimental-numerical technique," J. of Composite Materials, vol. 14, pp. 342-350, Oct. 1980.

12. Prabhakaran, R. "Photoelastic investigation of bolted joints in composites," Composites, pp. 253-256, July 1982.

13. Daniel, I. M., Niro, T. and Koller, G. M., "Development of orthotropic birefringent materials for photoelastic stress analysis," NASA Contractor Report 165709, May 1979.

14. Berghaus, D. G. "Overdetermined photoelastic solutions using least squares," Experimental Mechanics, vol. 13, no. 3, p. 97-104, 1973.

15. Chandrashekhara, K. and Jacob, K. A., "A numerical method for separation of stresses in photo-orthotropic elasticity," Experimental Mechanics, vol. 18, no. 2, pp. 61-66, 1978.

16. Bickley, W. G. "The distribution of stress round a circular hole in a plate," Phil. Trans. Royal Society (London) vol. 227A, pp. 383-415, July 1928.

17. Nisida, M. and Saito, H. "Stress distributions in a semi-infinite plate due to a pin determined by interferometric method," Experimental Mechanics, vol. 6, no. 5, pp. 273-279, May 1966.

18. Crews, J. H., Hong, C. S., and Raju, I. S. "Stress-concentration factors for finite orthotropic laminates with a pin-loaded hole," NASA TP 1862, May 1981.

19. de Jong, Th., "Stresses around a hole in an elastically orthotropic or isotropic plated loaded through a pin which moves without friction in a hole," (in Dutch) Report LR-223, Aerospace Department, Delft University of Technology, The Netherlands, July 1976.

20. de Jong, Th., "Stresses around pin-loaded hole in elastically orthotropic or isotropic plates," J. of Comp. Materials, vol. 11, pp. 313-331, 1977.

21. Hyer, M. W. and Liu, D., "An assessment of the accuracy of orthotropic photoelasticity," Proceedings of the Annual Spring Meeting, Society of Experimental Stress Analysis, 14 Fairfield Drive, Brookfield Center, CT 06805, pp. 248-253, 1983.

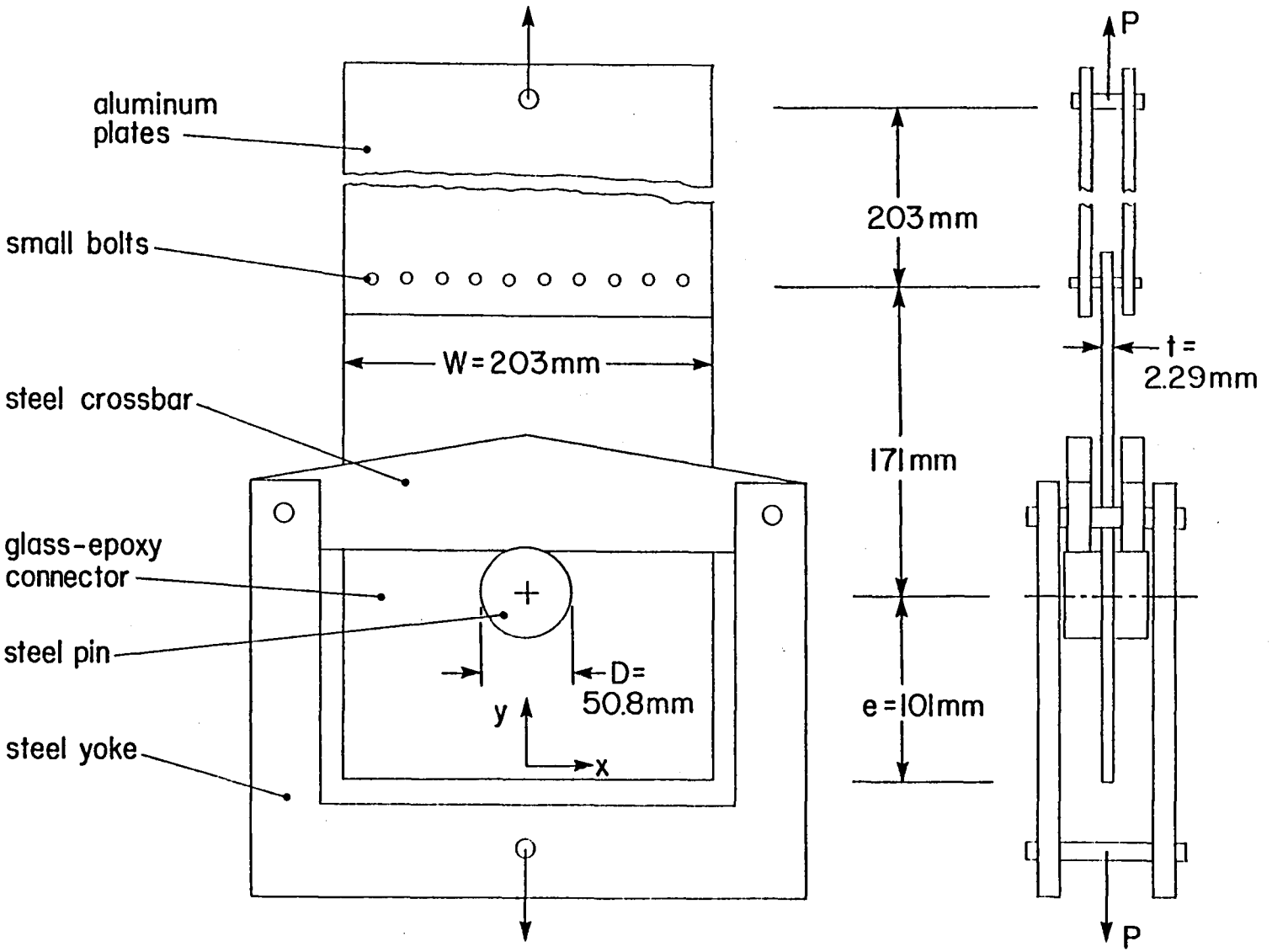

Fig. 1 Connector and loading apparatus.

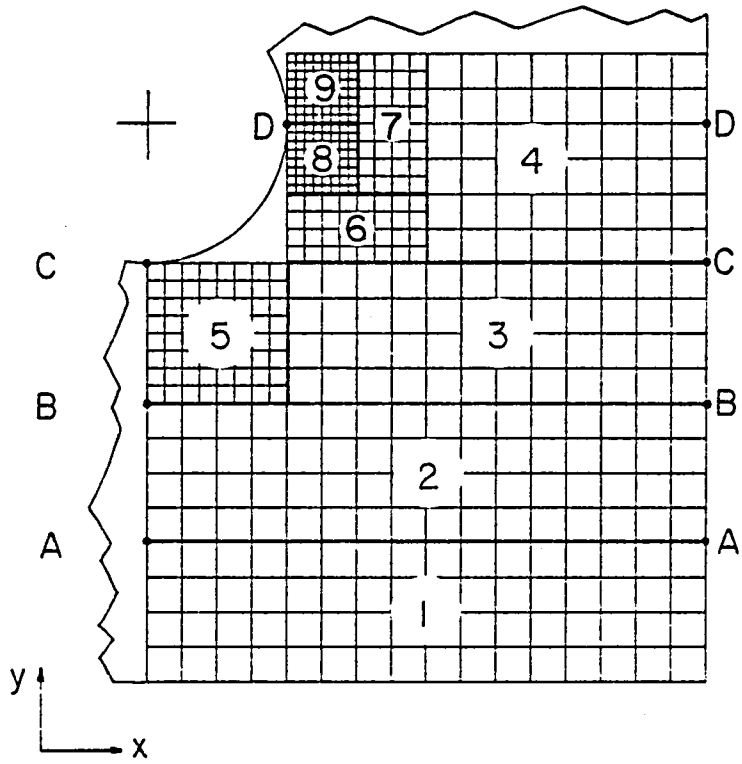

Fig. 2 Rectangular finite-difference grid.

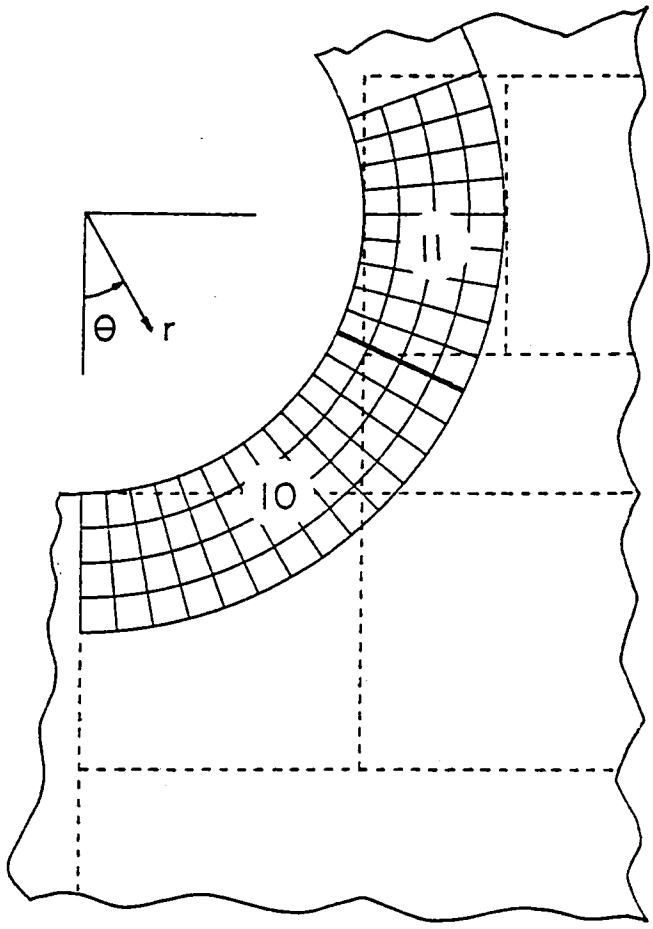

Fig. 3 Polar finite-difference grid.

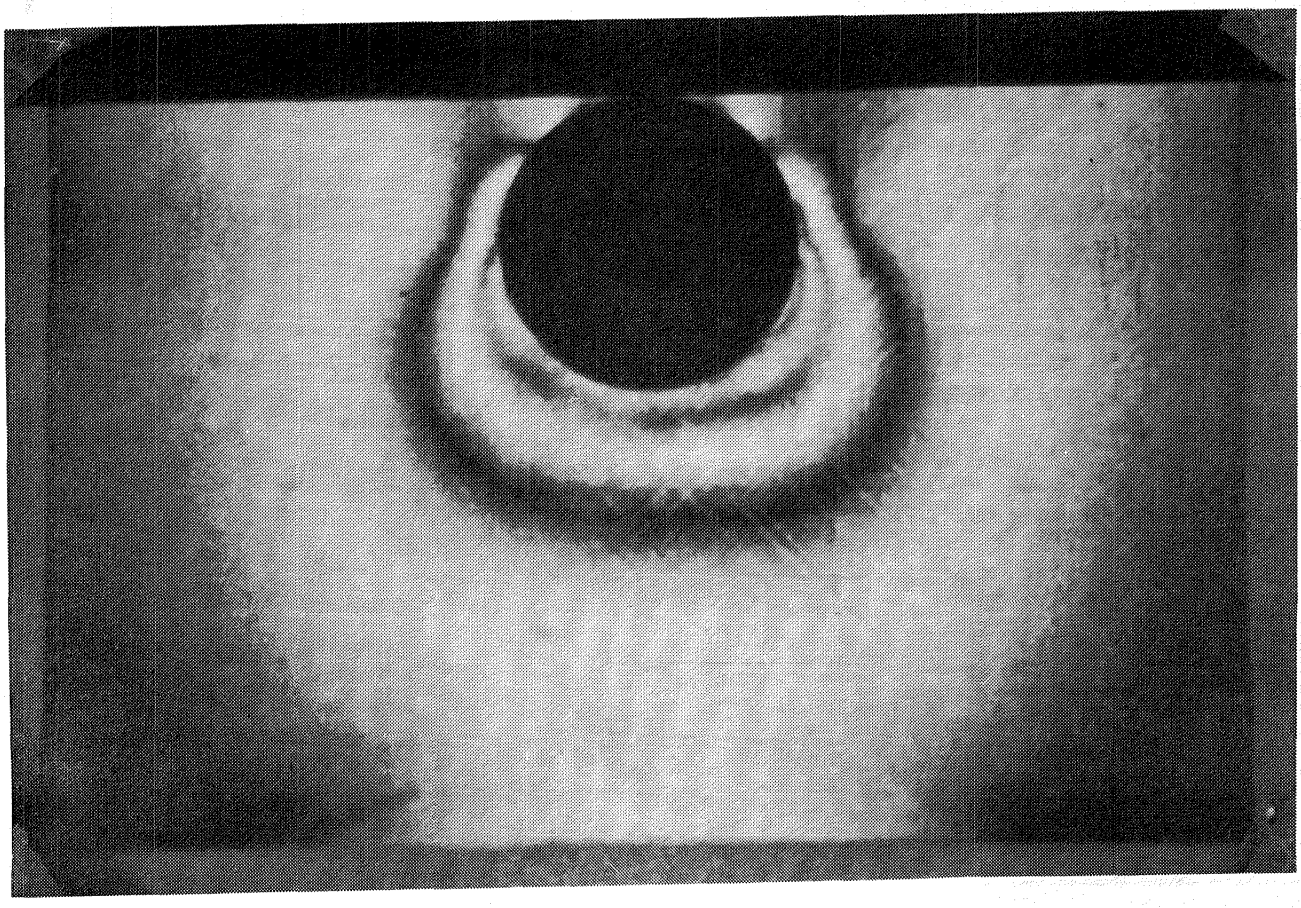

Fig. 4 Darkfield isochromatic fringe pattern, load = 7700 N (1730 lb.).

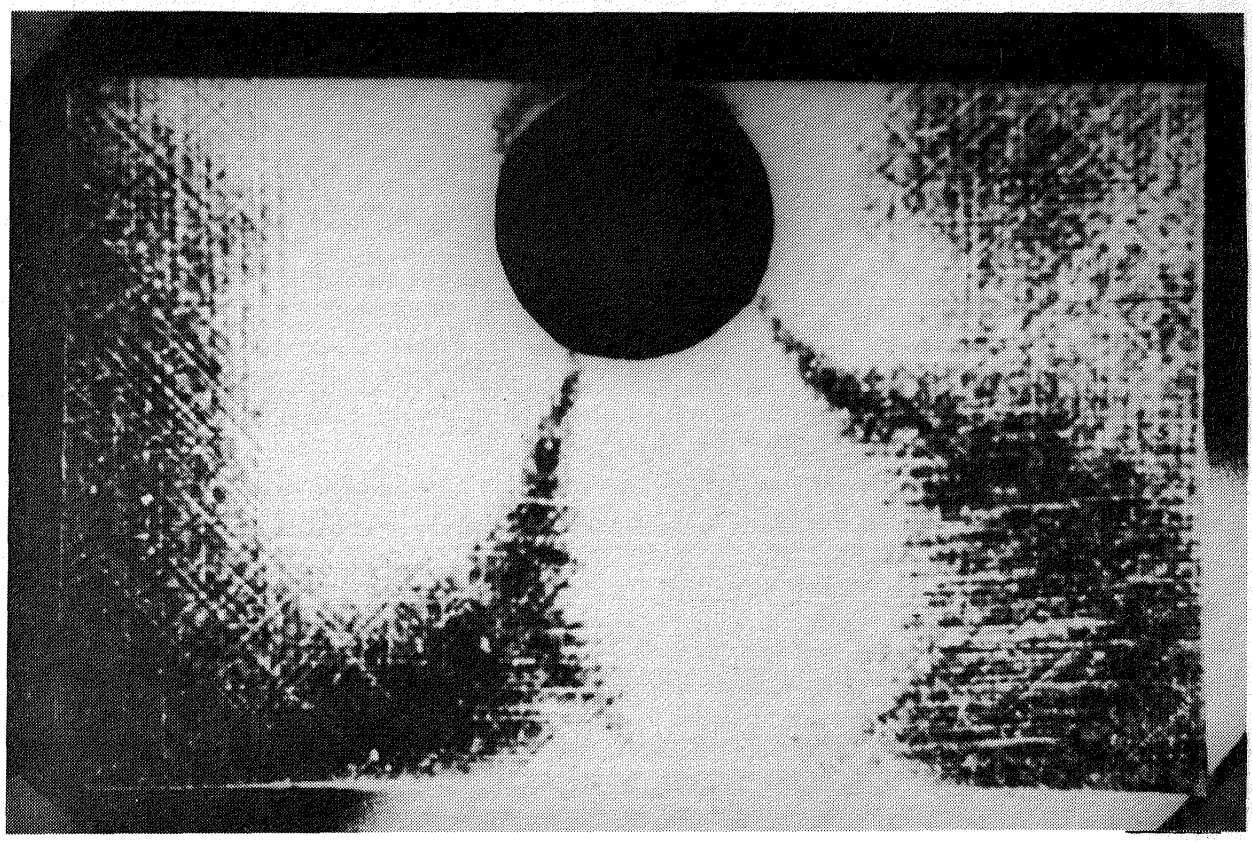

Fig. 5 Isoclinic fringe pattern, $\theta = 20°$
load = 7700 N (1730 lb.).

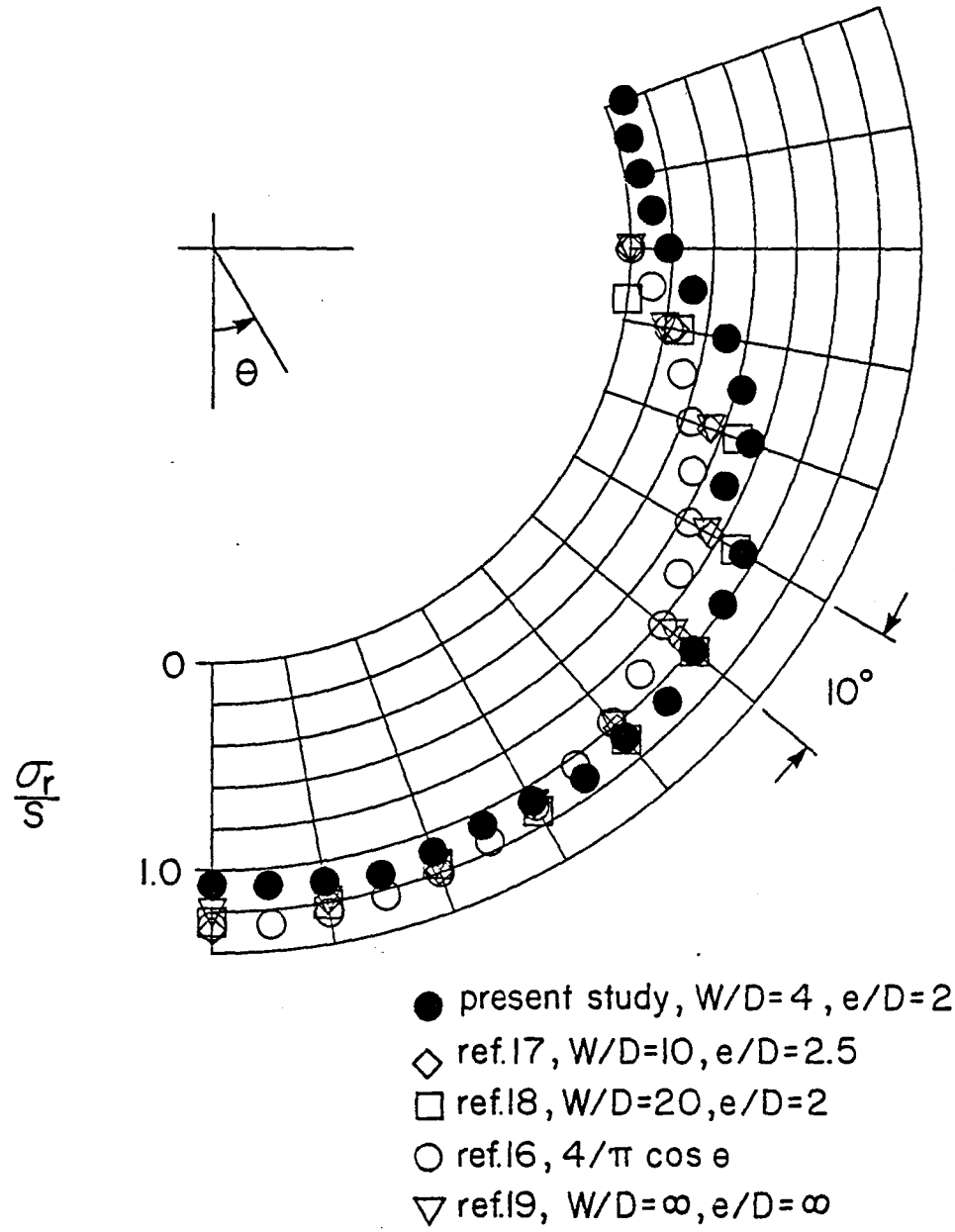

Fig. 6 Radial stresses around hole edge.

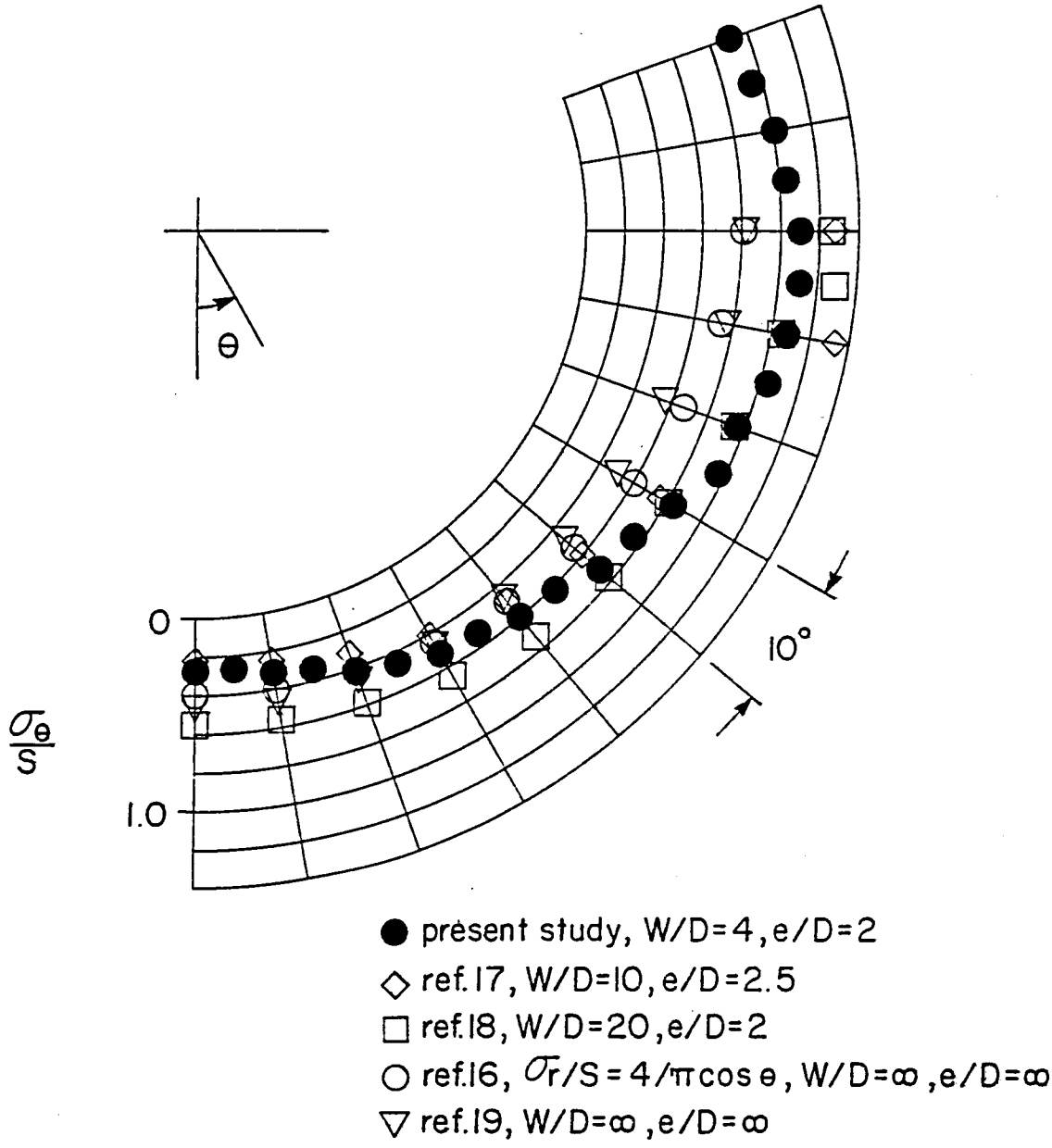

Fig. 7 Circumferential stresses around hole edge.

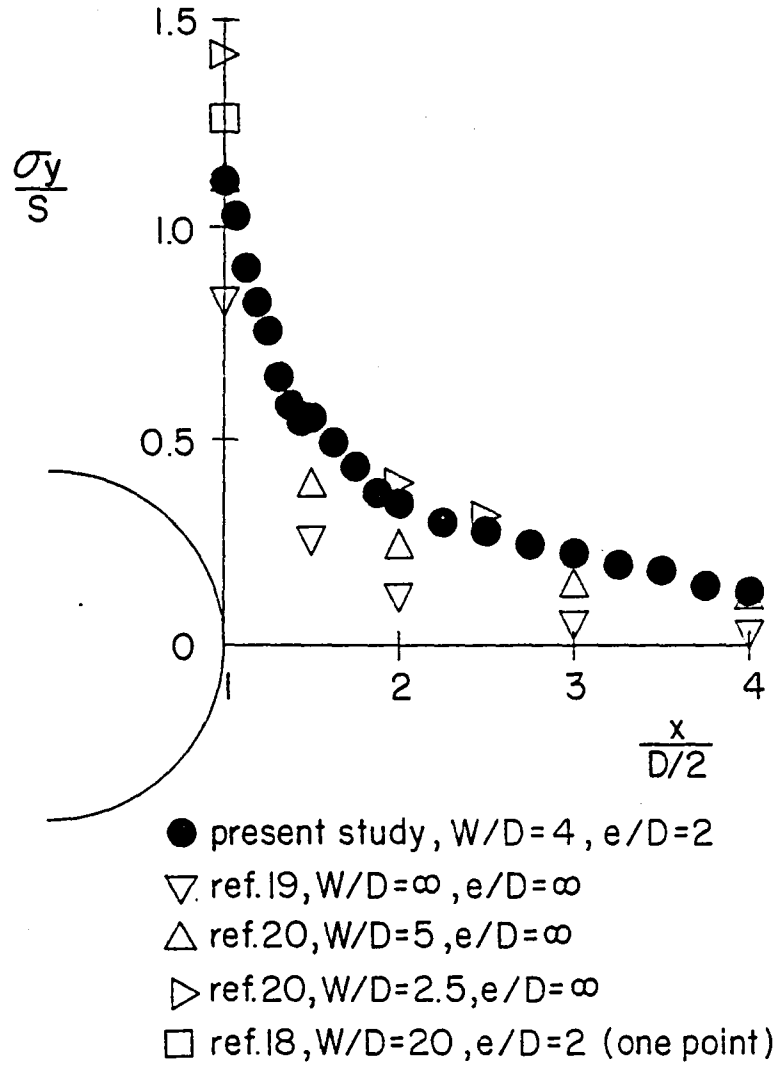

Fig. 8 Net-section tensile stresses.

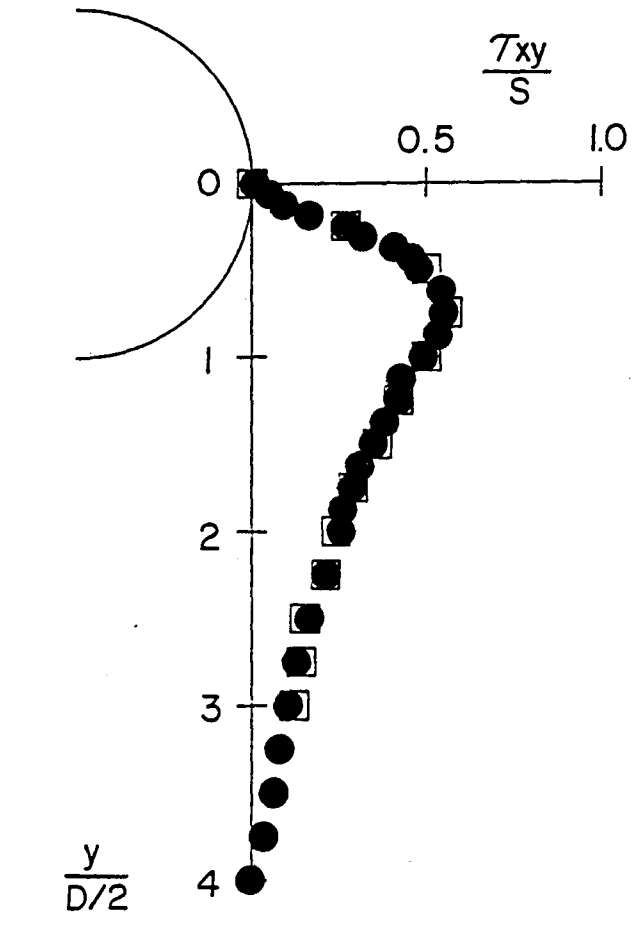

Fig. 9 Shear-out stresses below hole.

1. Report No.	2. Government Accession No.	3. Recipient's Catalog No.
NASA CR-172135		

4. Title and Subtitle	5. Report Date
Stresses in a Quasi-Isotropic Pin Loaded Connector Using Photoelasticity	August 1983
	6. Performing Organization Code

7. Author(s)	8. Performing Organization Report No.
Michael W. Hyer Dahsin Liu	
9. Performing Organization Name and Address	10. Work Unit No.
Department of Engineering Science and Mechanics Virginia Polytechnic Institute and State University Blacksburg, VA 24061	
	11. Contract or Grant No. NSG-1621
12. Sponsoring Agency Name and Address	13. Type of Report and Period Covered contractor report 3/16/82 - 3/15/83
National Aeronautics and Space Administration Washington, D.C. 20546	14. Sponsoring Agency Code 505-42-23-03

15. Supplementary Notes The research effort which led to the results in this report was financially supported by the Structures Laboratory, USARTL (AVRADCOM). The Langley Technical Monitor was Donald J. Baker, Structures Laboratory, USARTL (AVRADCOM).

16. Abstract

Birefringent glass-epoxy and a numerical stress-separation scheme are used to compute the stresses in the vicinity of a pin-loaded hole. The radial and circumferential stresses at the hole edge, and the net-section and shear-out stresses are computed. The numerical and experimental results of other investigators are compared with the computed stresses. The fixture used to load the connector is discussed and typical isochromatic and isoclinic fringe patterns are presented. The stress-separation scheme is briefly discussed.

17. Key Words (Suggested by Author(s))	18. Distribution Statement
orthotropic photoelasticity, pin-loaded connectors, glass-epoxy connectors, stress concentration factors, composite laminates bolted joints	unclassified - unlimited subject category 39

19. Security Classif. (of this report)	20. Security Classif. (of this page)	21. No. of Pages	22. Price
unclassified	unclassified	23	A02

End of Document